This is the accepted manuscript made available via CHORUS. The article has been published as:

Strongly Modified Spontaneous Emission Rates in Diamond-Structured Photonic Crystals

Matthew R. Jorgensen, Jeremy W. Galusha, and Michael H. Bartl

Phys. Rev. Lett. **107**, 143902 — Published 26 September 2011

DOI: 10.1103/PhysRevLett.107.143902

Strongly modified spontaneous emission rates in diamond-structured photonic crystals

Matthew R. Jorgensen, Jeremy W. Galusha, and Michael H. Bartl*

Department of Chemistry, University of Utah, 315 S 1400 E, Salt Lake City, Utah 84112

* To whom correspondence should be addressed to: M.H.B. (bartl@chem.utah.edu).

Abstract. *The spontaneous emission decay dynamics of nanocrystal quantum dots embedded into biotemplated titania photonic crystals with a diamond-based lattice are investigated. Modification of the decay rate of quantum dot emission over wide frequency bandwidths in the visible by the photonic crystals is observed. Frequency-dependent analysis reveals both inhibition and enhancement of emission with a radiative lifetime variation by more than a factor of ten.*

The dynamics of radiative transitions are directly proportional to the photonic density of states (DOS), according to Fermi's Golden Rule [1]. Given the pivotal role of radiative processes in solar energy conversion, solid-state lighting and lasing, along with quantum information processing, strategies to manipulate the radiative DOS over broad frequency ranges are of paramount technological importance. A central tenet in quantum electrodynamics is that the photonic DOS and thus the dynamics of spontaneous emission can be manipulated in the presence of specifically engineered environments [1-7]. Prime examples of such environments are three-dimensional (3D) periodically ordered crystal structures with lattice parameters comparable to the photon wavelength of interest. Due to this periodic variation of the refractive index, these materials, termed photonic crystals

(PCs), possess direction-dependent energy dispersion of photonic states (band structures) with directional photonic stopgaps (PSGs) and, under certain circumstances, overlap of all directional PSGs into a complete bandgap [8-15]. The band structure properties of these materials cause significant modifications in the DOS distribution [16], and importantly, compared to other DOS-modifying media such as optical microcavities [6,7], modifications occur over large bandwidths ($\Delta\omega/\omega$ of up to tens of percent) and are a bulk effect and thus not limited to small cavity volumes.

While such broadband modification of spontaneous emission has been demonstrated at infrared wavelengths in 2D [17] and 3D [14,15] photonic crystals, experimental studies at visible frequencies have been limited by the difficulty of fabricating PC structures that strongly modify the photonic DOS distribution. PCs mainly used at visible frequencies are so-called inverse-opals [18-21]. While inverse-opal PCs operating at visible frequencies have a 3D periodic lattice, unfortunately, they possess only non-overlapping single-directional PSGs and therefore cause only modest DOS modification [22,23]. PC structures with much stronger impact on the photonic DOS distribution would be those with diamond-based lattices [24-26]. In these lattices overlap of multiple PSGs occurs in the low frequency range (between the second and third optical band) for dielectric lattices with even only modest refractive indices [24]. However, in contrast to infrared PCs, difficulties of fabricating diamond-based PCs with lattice constants at visible wavelengths have kept them out of reach—until recently, when we discovered that the striking coloration of various weevils is the result of light reflecting from biopolymeric chitin PCs with a diamond-based lattice structure [27,28]. Moreover, these biopolymeric

structures can be used as molds for creating high-dielectric replicas, including the first PC with structural and dielectric properties for which calculations revealed a complete bandgap in the visible [29]. In this paper, we experimentally study excited state dynamics of photon sources placed inside such diamond-based PC lattices. We show that these photonic structures strongly modify the spontaneous emission dynamics of incorporated nanocrystal quantum dot (QD) emitters, resulting in unprecedented emission decay enhancement and inhibition by factors larger than ten.

Many butterflies and beetles obtain their coloration from elaborate 3D biopolymeric structures, including opal, gyroid and diamond-based lattices, incorporated into wing and exoskeleton scales [30,31]. The high-dielectric titania PCs with a diamond-based lattice used in this study were replicated from biopolymeric chitin scales of the beetle *Lamprocyphus augustus* [27], using our double-imprint sol-gel chemistry-based biotemplation method [29]. A typical scanning electron microscopy (SEM) image and the reconstructed 3D model of the ABC-stacked air-cylinder lattice in a nanocrystalline titania matrix (refractive index of ~2.2-2.3) is shown in Fig. 1(b). The corresponding photonic band structures and DOS distributions are shown in Fig. 1(a) and were calculated using the MIT photonic bands package [32] and our own program [33] based on the work by Busch and John [16]. The defining feature is strong overlap of multiple low-frequency PSGs, including the formation of a narrow complete bandgap of about 2.5 percent gap-width-to-mid-gap ratio. This results in a significant modification of the DOS distribution with strong depression of DOS in the overlap region and enhancement at the edges [Fig. 1(c)]. To study the impact of these DOS variations on excited state dynamics,

we analyzed the spontaneous emission decay rates of embedded CdSe/ZnS core-shell QD light sources ("eviDots" purchased from *Evident Technologies*). QDs with photoluminescence (PL) emission band positions overlapping with different parts of the photonic band structures were infiltrated into the PC samples by drop-casting from a 9:1 hexane/octane solution (9×10^{-9} M) [22]. The functionalized PC samples were then placed in a quartz cell under argon atmosphere to avoid photo-oxidation and mounted on a computer-controlled 3D nanomotion stage for optical micro-reflectance and time-correlated single photon counting (TCSPC) emission measurements.

Due to the inherent local inhomogeneity of biological/biotemplated structures [27,28], it is of great importance to inspect the sample quality by optical microscopy and micro-reflectance spectroscopy prior to determining the spontaneous emission decay rates of QDs at various locations inside the PCs. This was done by an optical set-up with a beam splitter/dichroic mirror combination to overlay a collimated white light source and the 405 nm line of a picosecond diode laser (Becker & Hickle BDL-405, 20 MHz repletion rate). Both beams were focused onto the sample with a 50x extra-long working distance objective (N.A. 0.55). The reflectance properties of each PC sample were first mapped out under white light illumination and at least ten spots per sample were chosen for spontaneous emission decay rate investigation. For this, the white light was blocked and the QDs were excited by the 405 nm line of the diode laser. The light emitted from the QDs was collected by the same microscope objective, directed into a spectrometer (Princeton Instruments SpectraPro 2300i), dispersed by a grating (600 grooves/mm) and detected by a thermoelectrically cooled single photon counting detector (Hamamatsu

Photosensor, H7422p). Spontaneous emission decay curves were collected over a 50 ns time window at a 12 ps time resolution.

Typical spontaneous emission decay curves for QDs located within the high-dielectric titania PCs with a diamond-based lattice are given in Fig. 2(a). Even a merely qualitative comparison of the decay curves for emission frequencies inside and outside of overlapping PSGs shows the strong impact of the PC. Not only does the PC band structure significantly alter the QD emission decay behavior, but it also results in strongly non-exponential decay behavior. The latter is the direct result of ensemble emission of randomly located light sources within the PC and displays the strong variation of the local photonic DOS [23,24]. This factor needs to be considered for quantitative decay curve analysis and choosing a physically meaningful model describing the local photonic DOS distribution is therefore of great importance for extracting relevant spontaneous emission rates from QD decay curves from within PCs. The problem of analyzing spontaneous emission from within PCs has been treated previously in the context of inverse opals by Nikolaev et al. [23], who recommended a log-normal distribution of decay rates. This distribution accounts for the variable local DOS experienced by the emitters while limiting the number of free fitting parameters. The maximum of the log-normal distribution represents the most probable rate of decay, while the distribution width relates to the variability of the local DOS over the entire unit cell. Here, a broad distribution width indicates that emitters experience the strong variation of local DOS present on the photonic structure's interior walls.

Quantitative QD emission decay curve analysis using the log-normal distribution fitting procedure revealed the immense impact of the PC. Average QD emission decay rates were obtained by measuring several different local positions inside the PC at a particular frequency. Within the predicted frequency zone of greatest inhibition (the simultaneous overlap of different PSGs) the QD emission decay was reduced by factors of more than six, resulting in a dramatic increase in the radiative lifetime to values reaching 100 ns inside the bandgap [Fig. 2(a)]. We obtained average QD emission decay rates of 0.068 ± 0.009 ns^{-1} (corresponding to a lifetime range of 13-18 ns) at frequencies far outside the inhibition zone. Inside the bandgap zone the decay rate of the same QDs decreased to values of 0.012 ± 0.002 ns^{-1} (lifetime range of 71-100 ns). In addition, the decay rate log-normal distribution width narrowed from 0.19-0.21 ns^{-1} to 0.064-0.076 ns^{-1}. This is indicative of a reduced overall DOS, since contribution to the local DOS from several directions is eliminated, as was suggested by Nikolaev and co-workers [23].

To put these inhibition results obtained from diamond-based PC structures in perspective and obtain an independent baseline, we fabricated inverse opal PCs consisting of the same nanocrystalline titania framework as the bioreplica. For this, polystyrene opal templates were fabricated by self-assembly [34] and converted into inverse opals using the same titania sol infiltration and processing method as for the bioreplica [29]. Two important results were obtained from the inverse opal study. Firstly, using the same QDs as for the previous experiments as light sources we found an inhibition of their emission by a factor of about two inside the inverse opal Γ-L PSG [Fig. 2(a)] and a reduction in the distribution width. The inhibition findings in titania inverse opals agree very well with

previously reported results [22,23]. This comparison— using the same light sources in both PC lattice types—provides clear evidence of the superiority of the diamond-based structure over inverse opal structures and points out the importance of several overlapping PSGs. Secondly, the decay rates of QD emission occurring outside any PSGs of the titania inverse opal PC gave values in the same range (13-17 ns) as we found for the titania bio-replica samples outside PSG regions. This finding is of great importance, since the framework of both PCs consists of the same sol-gel-derived titania material, and thus provides a valuable baseline. For the following analysis we therefore used titania inverse opal samples with PSG positions far away from the QD emission as an important additional control system for evaluating a baseline of QD radiative decay behavior that is not directly influenced by the PC-induced DOS variations.

To map the DOS variation of the diamond-based titania PC over a broad frequency range we systematically analyzed QD decay rate behavior over a large portion of the band structure, from 16,000 to 20,000 cm^{-1}. Decay rate measurements in the high frequency regime (at and above the PSG/edge range) were also attempted. However, for CdSe/ZnS QDs with emission frequencies above 20,000 cm^{-1} the emitting $1S_e$ electronic energy level moves above the titania conduction band (located at -3.9 eV below vacuum) [35]. This leads to strong QD-to-titania charge transfer [35,36]. In fact, the QD emission intensity decreased rapidly as we approached frequencies exceeding 19,000 cm^{-1} and QD emission completely disappeared beyond 20,000 cm^{-1}. Interestingly, the onset of charge transfer also seems to compensate the calculated increase in DOS in this regime, resulting in lower decay rates than predicted (see also Supplemental Material). Nevertheless,

reference baseline-normalized decay rate averages of QD emission within the 16,000 to 20,000 cm^{-1} frequency range (Fig. 2(b)) give some important insights into the emission decay control by a real PC. Both strong inhibition over a broad frequency range (>10 percent bandwidth) and enhancement within the narrow range of predicted DOS increase at the low-frequency bandedge were experimentally observed. Radiative lifetimes from 8 ns (enhancement region) to up to 100 ns (inhibition region) were obtained, spanning an unprecedented decay variation by a factor larger then ten.

The strong modification of spontaneous emission dynamics in diamond-based PCs highlights the superiority of PC lattices with strong overlap of multiple PSGs—in contrast to only a single PSG in inverse opals. Interestingly, we found that the decay rates stayed at very constant values within the entire region of overlap of multiple PSGs, including the narrow range of the calculated complete bandgap. Since the calculated complete gap is most likely too narrow to stay open in a real PC sample, we conclude that overlap of multiple PSGs, but not necessarily the complete bandgap, is responsible for the observed strong inhibition of excited state dynamics. The larger decay rate variations across different sampling spots (hence larger standard deviations) at the low frequency range of the inhibition region are most likely caused by the presence of PSG/edge combinations.

We further examined the finding that co-presence of multiple PSGs is the decisive factor in strong inhibition of spontaneous emission, by directly studying the properties of the biopolymeric PC structures, which consist of the rather low refractive index compound

chitin (about 1.5) [38]. Due to this low refractive index of the diamond-based lattice, this biological PC is far from opening a complete bandgap. Nevertheless, our photonic band structure calculations revealed overlap of multiple low-frequency PSGs [Fig. 3(a)]. To test the effect of these overlapping PSGs on the spontaneous emission decay behavior, we performed similar experiments as described above by embedding QDs into the biopolymeric PCs [39] and analyzing their spontaneous emission decay behavior. Indeed, we found strong inhibition of emission decay by a factor of two for emission inside the predicted zone of greatest DOS inhibition [Fig. 3(b)] with averaged inhibited radiative lifetimes as high as 39 ± 6 ns. Given the low refractive index of the biopolymeric PC structure the observed inhibition of spontaneous emission is remarkable, rivaling that of the best inverse opal PCs made from high-dielectric titania.

In conclusion, we experimentally demonstrated the strong impact of diamond-based photonic crystal lattices on spontaneous emission decay rates. The overlap of multiple PSGs in these structures efficiently modifies spontaneous emission dynamics of embedded light sources. Both inhibition and enhancement was observed with decay rate variations by a factor larger than ten, greatly exceeding previously used titania inverse opal photonic crystals. In addition, we showed even when made from compounds with refractive indices of only around 1.5, diamond-based lattices possess multiple overlapping PSGs and strongly affect spontaneous emission dynamics—a finding that further emphasizes the superiority of diamond-based lattices [24-26]. A multitude of functional dielectrics, including optoelectronically and piezoelectrically active polymeric materials, fall in this range, paving the ground for externally-tunable broadband control

of excited state dynamics in bulk materials. Our findings should therefore be of high relevance for future PC design—particularly for light-localization and quantum coherence based applications that require strongly inhibited radiative decay.

Acknowledgments. Allocation of computer time from the Center for High Performance Computing at the University of Utah is acknowledged. This research was partially funded by the National Science Foundation under Award No. ECS-0609244, a DuPont Young Professor Grant, and a Synergy grant and start-up funds from the University of Utah.

References

[1] R. Loudon, *The Quantum Theory of Light* (Oxford University Press, New York, 2000).

[2] M. O. Scully, M. S. Zubairy, *Quantum Optics* (Cambridge University Press, Cambridge, 1997).

[3] M. Woldeyohannes and S. John, J. Opt. B **5**, R43 (2003).

[4] E. Yablonovitch, Phys. Rev. Lett. **58**, 2059 (1987).

[5] P. Lambropoulos, G. M. Nikolopoulos, T. R. Nielsen, and S. Bay, Rep. Prog. Phys. **63**, 455 (2000).

[6] K. J. Vahala, Nature **424**, 839 (2003).

[7] K. Hennessy *et al.*, Nature **445**, 896 (2007).

[8] J. D. Joannopoulos, P. R. Villeneuve, and S. H. Fan, Nature **386**, 143 (1997).

[9] S. John, Phys. Rev. Lett. **58**, 2486 (1987).

[10] A. Blanco *et al.*, Nature **405**, 437 (2000).

[11] F. Garcia-Santamaria *et al.*, Adv. Mater. **19**, 1567 (2007).

[12] M. Maldovan, E. L. Thomas, and C. W. Carter, Appl. Phys. Lett. **84**, 362 (2004).

[13] Y. A. Vlasov, X. Z. Bo, J. C. Sturm, and D. J. Norris, Nature **414**, 289 (2001).

[14] M. H. Qi *et al.*, Nature **429**, 538 (2004).

[15] K. Aoki *et al.*, Nat. Photonics **2**, 688 (2008).

[16] K. Busch and S. John, Phys. Rev. E **58**, 3896 (1998).

[17] M. Fujita, S. Takahashi, Y. Tanaka, T. Asano, and S. Noda, Science, **308**, 1296 (2005).

[18] B. T. Holland, C. F. Blanford, and A. Stein, Science **281**, 538 (1998).

[19] G. Subramanian, V. N. Manoharan, J. D. Thorne, and D. J. Pine, Adv. Mater. **11**, 1261 (1999).

[20] J. Wijnhoven and W. L. Vos, Science **281**, 802 (1998).

[21] J. W. Galusha, C. K. Tsung, G. D. Stucky, and M. H. Bartl, Chem. Mater. **20**, 4925 (2008).

[22] P. Lodahl *et al.*, Nature **430**, 654 (2004).

[23] I. S. Nikolaev, P. Lodahl, A. F. van Driel, A. F. Koenderink, and W. L. Vos, Phys. Rev. B **75**, 115302 (2007).

[24] M. Maldovan and E. L. Thomas, Nat. Mater. **3**, 593 (2004).

[25] A. Moroz, Phys. Rev. B **66**, 115109 (2002).

[26] K. M. Ho, C. T. Chan, and C. M. Soukoulis, Phys. Rev. Lett. **65**, 3152 (1990).

[27] J. W. Galusha, L. R. Richey, J. S. Gardner, J. N. Cha, and M. H. Bartl, Phys. Rev. E **77**, 050904 (2008).

[28] J. W. Galusha, L. R. Richey, M. R. Jorgensen, J. S. Gardner, and M. H. Bartl, J. Mater. Chem. **20**, 1277 (2010).

[29] J. W. Galusha, M. R. Jorgensen, and M. H. Bartl, Adv. Mater. **22**, 107 (2010).

[30] M. Srinivasarao, Chem. Rev. **99**, 1935 (1999).

[31] A. E. Seago, P. Brady, J. P. Vigneron, and T. D. Schultz, J. R. Soc. Interface **6**, S165 (2009).

[32] S. G. Johnson and J. D. Joannopoulos, Opt. Express **8**, 173 (2001).

[33] See Supplemental Material for more details on photonic band structure and DOS calculations.

[34] S. H. Im, M. H. Kim, and O. O. Park, Chem. Mater. **15**, 1797 (2003).

[35] J. Jasieniak, *et al.*, Adv. Funct. Mater. **17**, 1654 (2007).

[36] P. V. Kamat, J. Phys. Chem. C **112**, 18737 (2008).

[37] L. Bechger, P. Lodahl, and W. L. Vos, J. Phys. Chem. B **109**, 9980 (2005).

[38] J. A. Noyes, P. Vukusic, and I. R. Hooper, Opt. Express **15**, 4351 (2007).

[39] M. R. Jorgensen, B. Yonkee, and M. H. Bartl, Proc. SPIE **8071**, 807109-1 (2011).

Figure Captions

FIG. 1 (color online). (a) Calculated photonic band structure for a diamond-based lattice of air cylinders surrounded by dielectric with refractive index of 2.2; shown is the low-frequency region around the overlapping PSGs. Calculations are based on scanning electron microscopy images of the titania PC lattice (a = 354±9 nm) used in this study (b). Inset in (b) shows the dielectric model for the band structure calculations. (c) Corresponding calculated DOS of PC lattice described in (a). See Supplemental Material

for details of photonic band structure and DOS calculation. Scanning electron microscopy images were adapted from reference 27.

FIG. 2 (color online). (a) Selected PL emission decay curves plotted on a normalized log scale of QDs embedded into various titania PCs. QD emission in the region of strong PSG overlap (solid line; calculated lifetime of 99±2 ns) and at the low-frequency bandedge (dotted; calculated lifetime of 8±1 ns) of the titania PC with a diamond-based lattice (for a full range of decay curves, see Supplemental Material). QD emission inside the titania inverse opal *Γ*-*L* PSG (dashed; calculated lifetime of 20±1 ns) and in the titania reference sample outside of any PSGs (dashed-dotted; calculated lifetime of 14±1 ns). Reported lifetimes reflect the peak of the log-normal distribution of the decay curve fitting. (b) Decay rates of QD spontaneous emission over a broad frequency range of the band structure of the titania PC with a diamond-based lattice, including regions of normal, enhanced and emission. All decay rates are given relative to the decay rates of the same QDs in a titania reference sample outside any PSGs. Vertical error bars indicate the variation of the measured lifetime over several spatial positions in the sample. Horizontal bars represent the spectral width over which the measurements were made.

FIG. 3 (color online). (a) Calculated photonic band structure for the biopolymeric (chitin) PC used in this study; shown is the low-frequency region with three overlapping PSGs. (b) PL emission decay curves plotted on a normalized log scale for QDs in the region of overlapping PSGs (top) and far away from any PSGs (bottom). The inset in (b) shows the calculated DOS for the biopolymeric (chitin) PC. Both decay curves were measured

at 18,350 cm^{-1} in two different isomorphic structures with different lattice constants. The reduced frequency positions are indicated by the two arrows and the width of the arrows resembles the lattice constant uncertainty of these biological photonic structures.

Figure 1

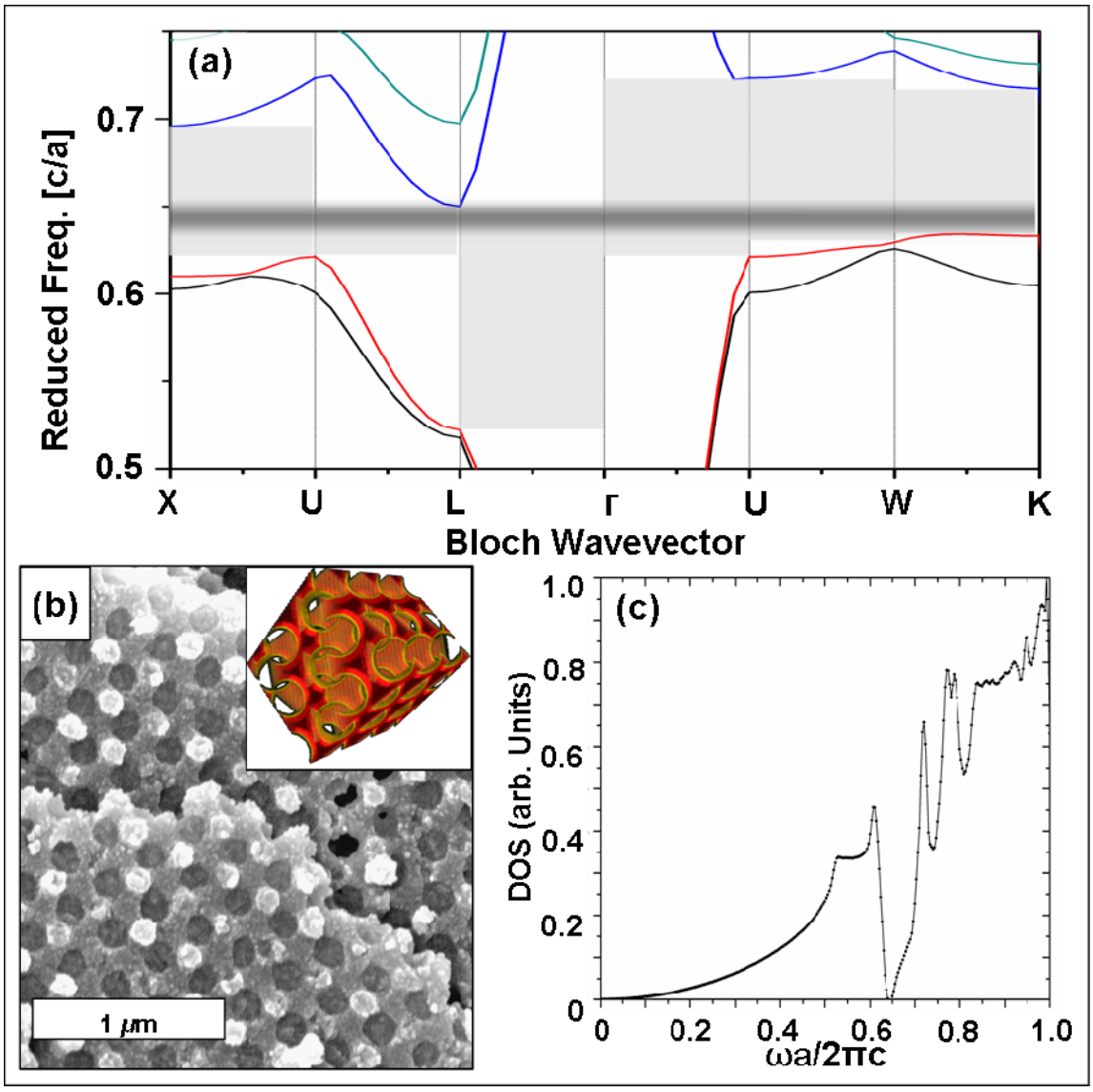
(a)
Reduced Freq. [c/a]
0.7
0.6
0.5
X
U
L
Γ
U
W
K
Bloch Wavevector
(b)
1 μm
(c)
DOS (arb. Units)
1.0
0.8
0.6
0.4
0.2
0
0
0.2
0.4
0.6
0.8
1.0
ωa/2πc

Figure 2

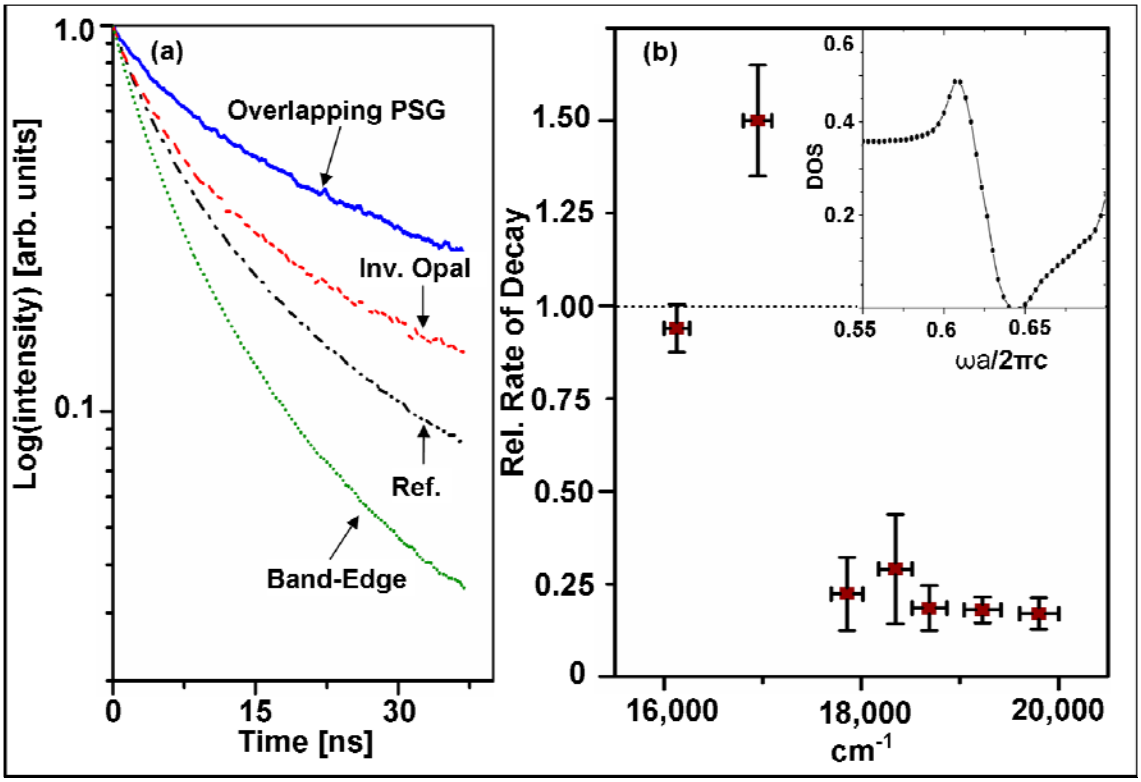
(a)
Overlapping PSG
Inv. Opal
Ref.
Band-Edge
Log(intensity) [arb. units]
1.0
0.1
0
15
30
Time [ns]
(b)
Rel. Rate of Decay
1.50
1.25
1.00
0.75
0.50
0.25
0
16,000
18,000
20,000
cm-1
DOS
0.6
0.4
0.2
0.55
0.6
0.65
ωa/2πc

Figure 3

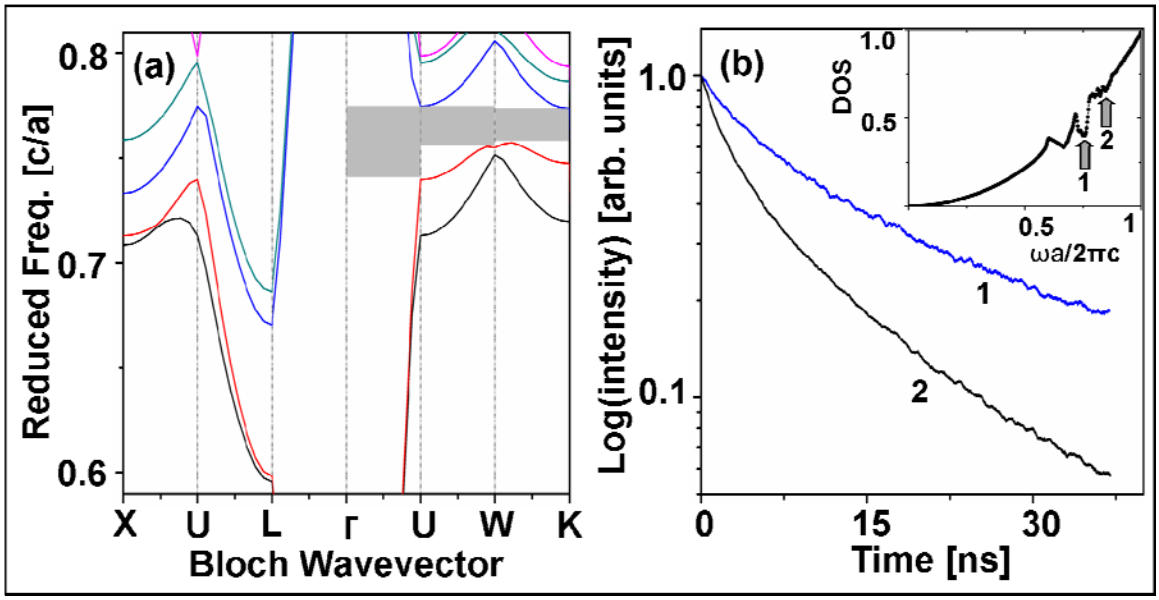
(a)
Reduced Freq. [c/a]
0.8
0.7
0.6
X
U
L
Γ
U
W
K
Bloch Wavevector
(b)
Log(intensity) [arb. units]
1.0
0.1
0
15
30
Time [ns]
1
2
DOS
1.0
0.5
0.5
1
ωa/2πc
1
2